NRIAG JOURNAL OF ASTRONOMY AND GEOPHYSICS
2021, VOL. 10, NO. 1, 387–396
https://doi.org/10.1080/20909977.2021.1979889

Integrated electromagnetic survey for groundwater exploration: case study at El-Minya, western desert of Egypt

Gad El-Qady, Hany Shaaban, Mohamed Abdel Zaher and Magdy Atya

Geomagnetic and Geoelectric Department, National Research Institute of Astronomy and Geophysics (Nriag), Cairo, Egypt

ABSTRACT

The determination of groundwater potentiality is one of the most significant challenges in hydro-geophysical research, especially in arid areas with limited water resources. A geophysical survey was carried out in the northwest of El-Minya Governorate to investigate the groundwater aquifer. A total of 20 controlled source audio-magnetotelluric (CSAMT) and 20 time domain electromagnetic soundings (TEM) were surveyed along two parallel profiles with station spacing varying between 500 and 2000 m. The CSAMT data was acquired using a hybrid source of low frequency band (0.1 Hz – 1 KHz) and standard high frequency band (10 Hz- 100 KHz). For the TEM survey, a coincident loop of side length of 50 m was used. The results of the integrated interpretation of both data sets (TEM and CSAMT) show a good consistency in the conductivity distribution. However, inspection of the results of the cross section indicates that two to three geoelectrical layers can be recognised in the subsurface medium. The area's water potentiality is divided into two levels: the first begins immediately beneath the rock cap at depths of over 50 m and reaches nearly 200 m in some spots. The second level begins at a depth of 250 m and continues to a depth of 500 m.

ARTICLE HISTORY
Received 9 May 2021
Revised 31 August 2021
Accepted 9 September 2021

KEYWORDS
Groundwater aquifer; csamt; tem; arid areas; el-minya governorate

1. Introduction

Western desert of Egypt extends for huge area and is characterised by lack of agriculture due to low availability of water. Recently, many interesting projects for the development of these areas had been considered. One of the most important places in Egypt that is promising for development plans, such as agricultural zones (back side of the western desert) and new urbans, is El-Minya Governorate. El-Minya is considered as a low tectonic depression of average depth 32–44 m with two high belts on the edges of the Nile Valley. The study area at the western part of the Nile Valley has elevation varying from 82 up to 130 m above sea level. The study area is situated at the north west of El-Minya Governorate (Figure 1) between latitudes 28.35° and 28.45° North and between longitudes 30.45° and 30.50° East.

Surface geophysical techniques can diminish hazard and pointless expenses by aiding the arrangement of wells in areas with the most extreme prospect to deliver sufficient amounts of water. These techniques have been utilised for years to effectively and monetarily conduct groundwater investigations. For examinations to profundities of around 500 m, the time domain electromagnetic (TDEM) technique was successfully utilised; in any case, at larger profundities, TDEM turns out to be strategically hard and less monetary (Amato et al. 2021; Mahmoud et al. 2021). In recent years, the magnetotelluric (MT) methods are more extensively used for deep groundwater exploration as they give monetary, stratigraphic, and structural features to depths reaching up to 3,000 m (Shaaban et al. 2016; Fornaciai et al. 2021; Grimm et al. 2021; Ye et al. 2021; Zhang et al. 2021).

The present geophysical surveys have been adopted to study the hydrogeological setting at El-Minya, Western Desert, Egypt, whereas the objectives of this study are to study the geologic and hydrologic setting to a considerable depth, identify the water bearing formations and the water table, delineate the reservoir dimensions and define the production spots and drilling recommendation.

2. Geological and stratigraphic settings

Geomorphologically, the study area consists of three main units from west to east: the limestone plateau, the elderly alluvial plain, and the early alluvial plain (Figure 2). For the most part of the study area, the land surface goes down delicately longitudinal way (towards the North), while the lateral slop towards the Nile (towards the East) is enormously high. The stratigraphy of El-Minya is mainly dominated by sedimentary rocks varying in age from tertiary and quaternary (Figure 2) (Abou Heleika and Niesner 2008; Ammar, A. I., et. al., 2021; El Ayyat, A. M.,

CONTACT Hany Shaaban hshaaban001@yahoo.com National Research Institute of Astronomy and Geophysics (Nriag), Helwan-11421, Cairo, Egypt

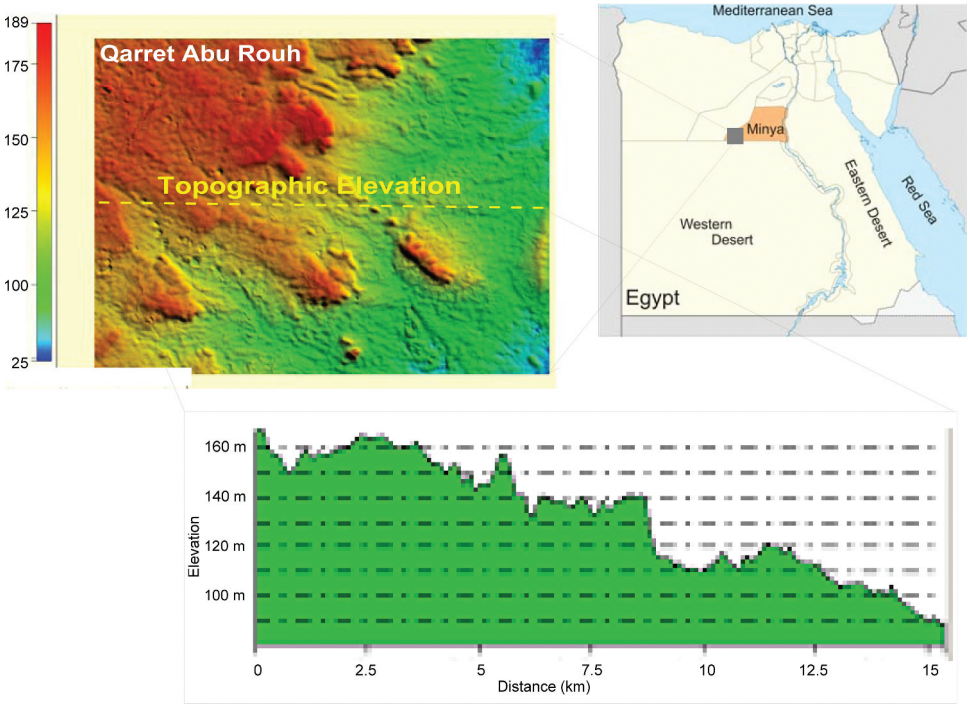

Figure 1. Location map of the study area exhibiting its main topography.

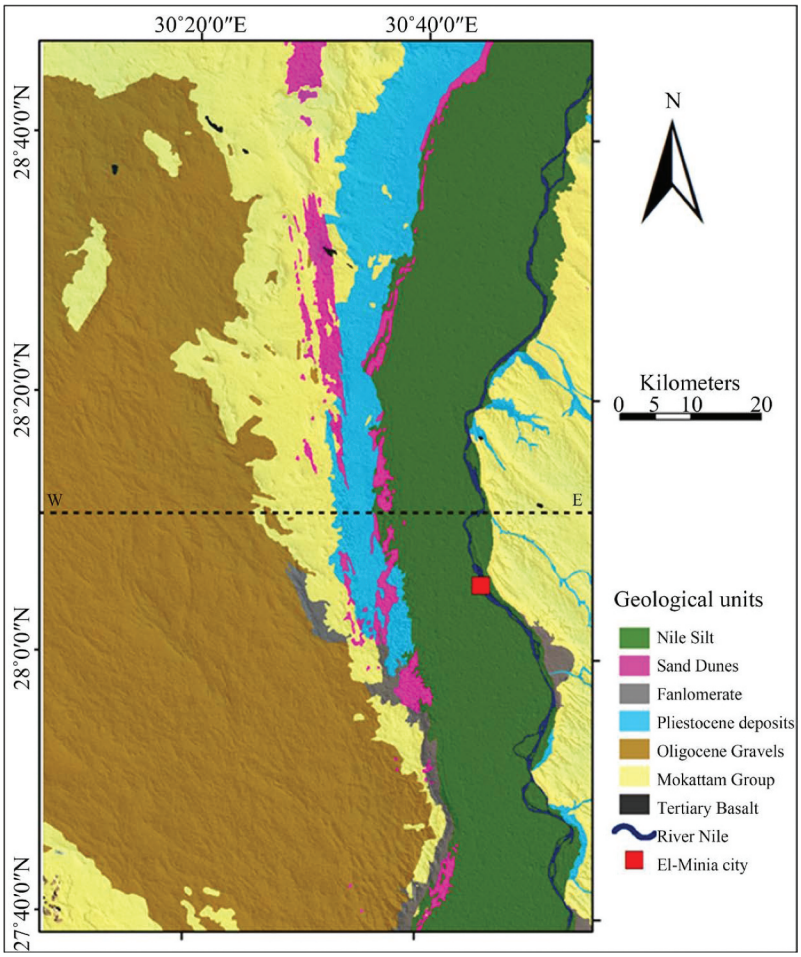

Figure 2. Geological map with geological cross-section (Line W-E) in El-Minya (see Figure 3), modified after (Abdel Moneim, et. al. 2016).

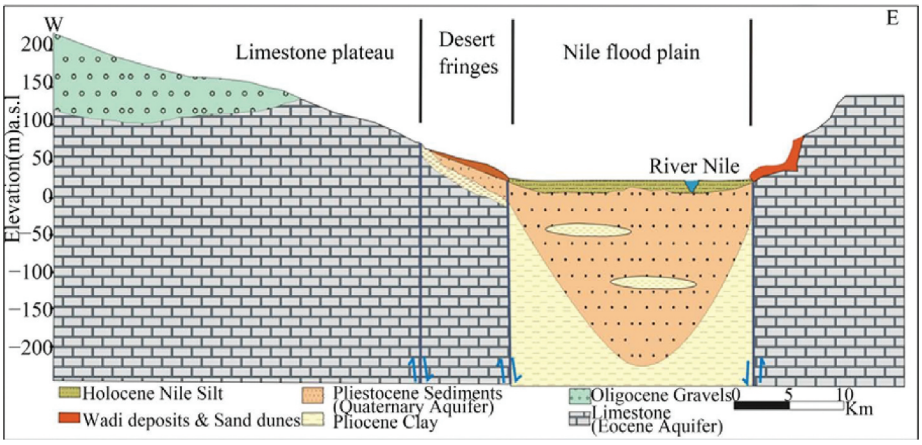

Figure 3. Hydrogeological cross-section in El-Minya, (Rigw, 1992).

2021; El-Rawy, M., 2021; Ismail, E. et. al. 2021). Samalut and El-Minya formations comprising essentially of limestone (Mokattam group) are one of the principle water bearing formations. It includes chalk and dense limestone with joints, fractures and fissures, which create channels of the groundwater framework (Said 1997). It was noticed that the tertiary volcanic basalt dykes interfered to the chalky limestone aquifer upgrade the interconnection of the fracture systems (Abou Heleika and Niesner 2008). Moreover, the Nile Valley is restricted by wrench faults that are parallel either to the Gulf of Suez or to the Gulf of Aqaba bearings. They are of normal type trending NW-SE. They play a great role in recharging the Middle Eocene Limestone Aquifer (Shabana 2010).

In the study area, groundwater is regarded as a portion of the provincial Nile Valley aquifer framework. Quaternary and Eocene aquifers are distinguished in the study area (Figure 3). The quaternary aquifer has a broad areal augmentation, particularly on the westward of the Nile Valley. Generally, the aquifer is composed of alluvial sediments of gravels and sands intercalated with clay lenses. This aquifer is covered by Holocene Nile silt and sandy clay reaching out into a semi-permeable to impermeable layer. The Quaternary aquifer has a huge expansion in the north–south bearing. It is restricted from the East and West, while it lies unconformable on Middle Eocene Limestone (RIGW, 1992; 2018). The thickness of the aquifer decreases from 200 m below the Nile to few metres near its margins (RIGW/IWACO 1989). On the other hand, the Middle Eocene limestone aquifer carries the Quaternary aquifer and superimposes the Nubian sandstone aquifer. The Eocene water-bearing formation possesses the outrageous eastward and westward of the study area. This aquifer corresponds to Samalut formation and is composed of fossiliferous limestone with marl and shale intercalations. Eocene limestone is cracked and is influenced by the faulting system (Said 1997).

3. Geophysical data

Two different geophysical methods have been used in this study, which is time domain electromagnetic (TEM) and hybrid-controlled source magnetotelluric (CSMT). The following section gives brief discussion for each of the techniques and data acquisition.

3.1. TEM data

The TEM technique is well appropriated for subsurface mapping of the highly conductive materials (Shaaban et al. 2016). It is an inductive tool that uses a DC transferred through a loop placed on the earth's surface. The DC current will generate a primary magnetic field that will spread out into the earth. When the DC is switched off, the primary magnetic field begins to decline with time. Based on Faraday's law, the decay of the primary magnetic field with time will generate eddy currents that move everywhere in the below conductors. The degree of variation of these currents and their identical secondary magnetic field rely upon the dimension and form of the subsurface conductors.

The *SIROTEM MK3* conductivity meter was used for measurements, applying the coincident loop configuration (Buselli and O`Neill, 1977) with a loop side length of 50 m. The composite mode through 35-time gates was used for recording the TEM data. The receiver coil records the changing rate of the magnetic field as a function of time (dB/dt) through the transient. These are transformed into resistivity against decay time, which will be converted later to be resistivity

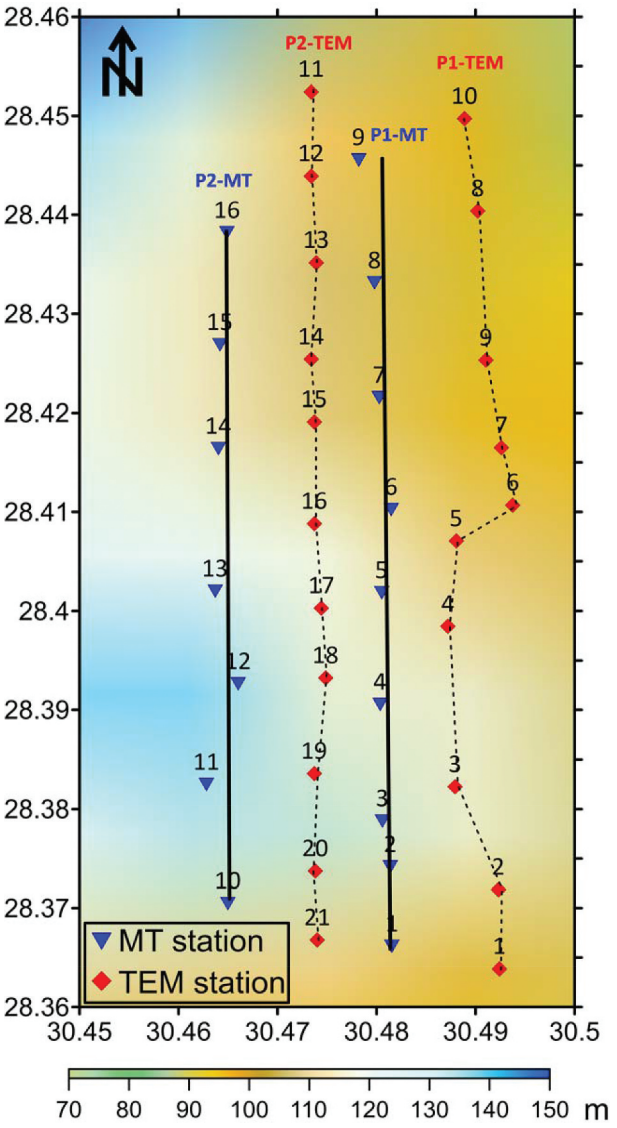

Figure 4. Location map of the MT and TEM sites projected on the DEM map of the study area.

against depth. The TEM data were recorded at 21 sites, about 1000 m apart, arranged along two north-south trending profiles, as shown in Figure 4.

3.2. CSAMT data

The MT strategy decides the electric conductivity earth model from estimations of natural varieties of the subsurface magnetic and electric fields over the wide range of frequency (Vozoff 1991). Controlled source MT (CSAMT/MT) is a hybrid technique that estimates subsurface electrical conductivity allocation by calculating time-dependent deviations of the natural magnetic and electric fields, as well as those resulting from electromagnetic waves of high frequency and tempting artificially sent (CSAMT).

The technique acquires the resistivity of subsurface bodies in two perpendicular directions with opposite electric dipoles (Ex and Ey) and magnetometers (Hx and Hy). As a rule, electric and magnetic fields are estimated to be both identical and contradictory to strike, hence providing CSAMT/MT a two-dimensional extent that is not accomplished by other techniques. CSAMT/MT field data comprise logarithmic schemes of apparent resistivity curves versus frequency. Subsurface resistivities can be determined with forward and inverse computer modelling programming by changing over the sounding curve data to modelled resistivity structure or layering beneath the measured site. The profundity of penetration is a component of both frequency and ground conductivity, since the profundity of signal penetration is contrarily identified with signal frequency.

CSAMT measurements have been conducted through 16 stations along two lines that oriented north-south moderately parallel to the trend of the Nile River. The station spacing is 1.5 km on average and varies between 0.5 and 3 km (Figure 4), and the measurements have been accomplished using a Stratagem instrument with two kinds of frequencies: high and low frequency, where high frequency data are used to investigate shallow depths and low frequency measured structures at greater depth.

4. Data processing

4.1. TEM data

TEM data were inverted in 1D using TEMIX XL 4 (1996) and ZondTEM (2016) programmes, assuming a layered-earth model (Figure 5). The observed data have fit the model responses in rms within 6%. The best-fitted model has been used to create two geoelectrical cross-sections along the profiles P1 and P2, as shown in Figures 6 and 7, respectively.

4.2. CSAMT data

Processing and interpretation of CSMT data are conducted by using WinGLink software (GEOSYSTEM SRI). As a result, noisy stations were eliminated from the database. Two modes were measured in MT data: high frequency mode ranges from 10 Hz to 100 kHz and low frequency mode is as low as 0.1 Hz. The first step in data handling is to merge MT data at various frequencies for the same MT station. Then, the merged data were utilised to calculate the elements of the impedance tensor, which is finally used for determining the apparent resistivities and phases.

Figure 8 shows examples of the apparent resistivity curves as well as their corresponding phase curves for sites in profiles 1 and 2. Nearly at all frequencies, the apparent resistivities are harmonious for the XY-and YX-parts with a small offset, showing a small static shift. The apparent resistivities in all MT sites increment in low frequencies that reflect the expanding resistivity with profundity. The motions in the

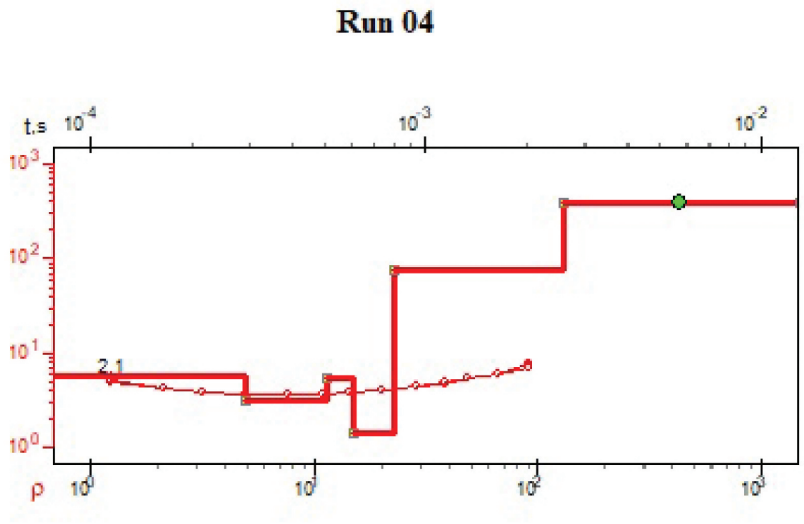

N	ρ	h	z
1	5.83	4.95	4.95
2	3.17	6.54	11.49
3	5.48	3.5	15.02
4	1.41	7.96	22.98
5	75.99	106.18	129.15
6	389.39		

Figure 5. Example of the TEM resistivity curve and its inverted model for station no. 4.

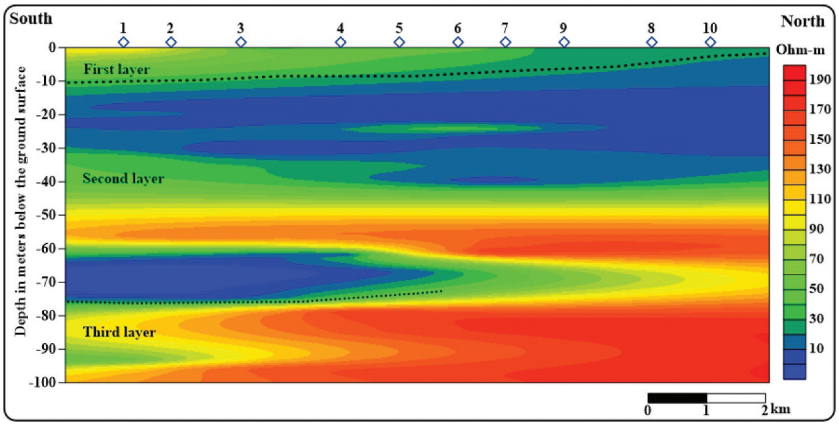

Figure 6. TEM cross section no. 1.

apparent resistivity above 0.1 Hz are because of the presence of resistive layer in the upper surface. The MT phases are additionally displaying these oscillations. The dispersion of the MT phase with frequencies is due to the subsurface structure that is not really 2D.

4.2.1. 1D and 2D inversion of MT Data

1D inversion of MT data was performed by employing the Bostick scheme (Bostick 1977). The Bostick transformation of MT data for some selected soundings is shown in Figure 9. The inversion was completed by accepting a model

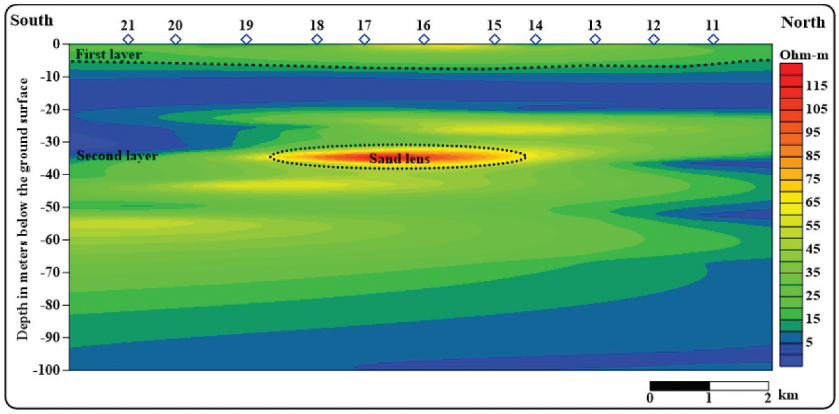

Figure 7. TEM cross section no. 2.

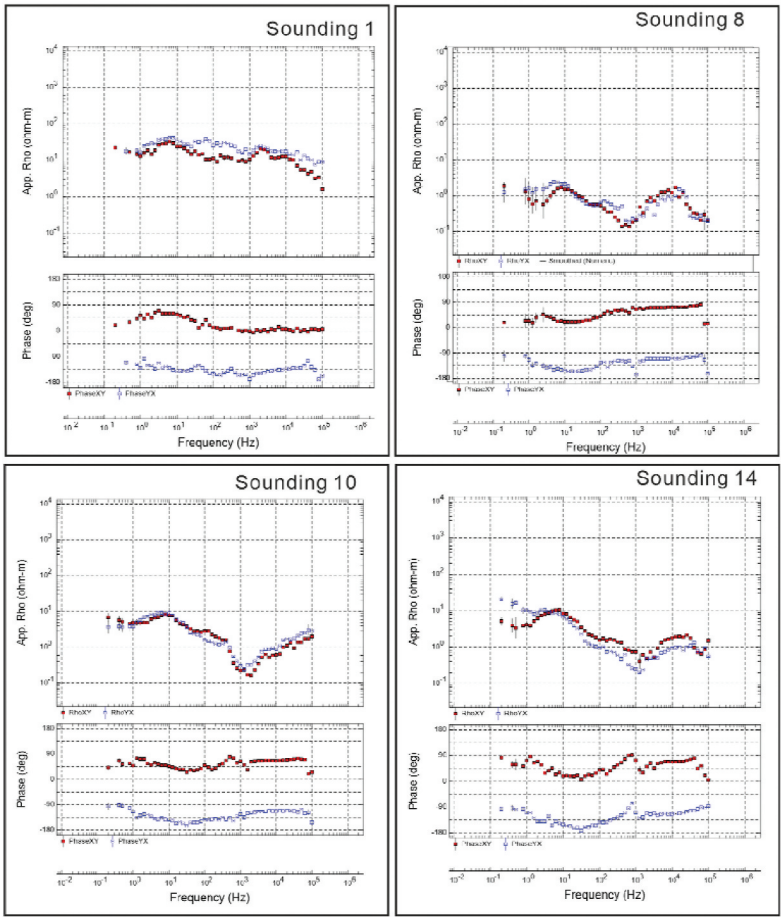

Figure 8. Examples of apparent resistivity and phase field curves for MT data.

comprising a base number of layers with different resistivity limits. This inversion scheme creates a close constant resistivity appropriation against depth (Bostick 1977). Consequently, the best fit between the field and computed data gives the best model. Soundings 3, 5, 6, 8 and 9 in profile 1 have same resistivity properties with depth, which indicate the equivalent subsurface strata underneath them. However, in sites 4 and 7, the resistivity curves show up high resistivity values at lower frequencies that demonstrate low conductive layers. Additionally, sites 15 and 16 in profile 2 demonstrate these high resistive layers.

2D inversion was also conducted on the two MT profiles using a code of 2D inversion REBOCC (Siripurnvaraporn and Egbert, 2000). For 2D inversion, the determinant apparent resistivities and phases are determined and used. The finished 2D models are shown in Figure 10 along profiles 1 and 2. In a homogeneous half-space, the starting model of

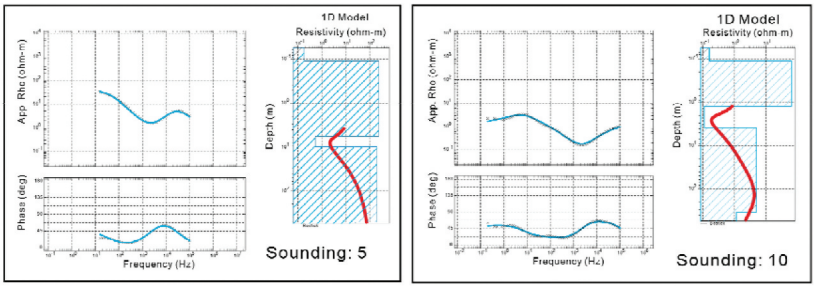

Figure 9. Examples of the 1D Bostick model for two MT sites.

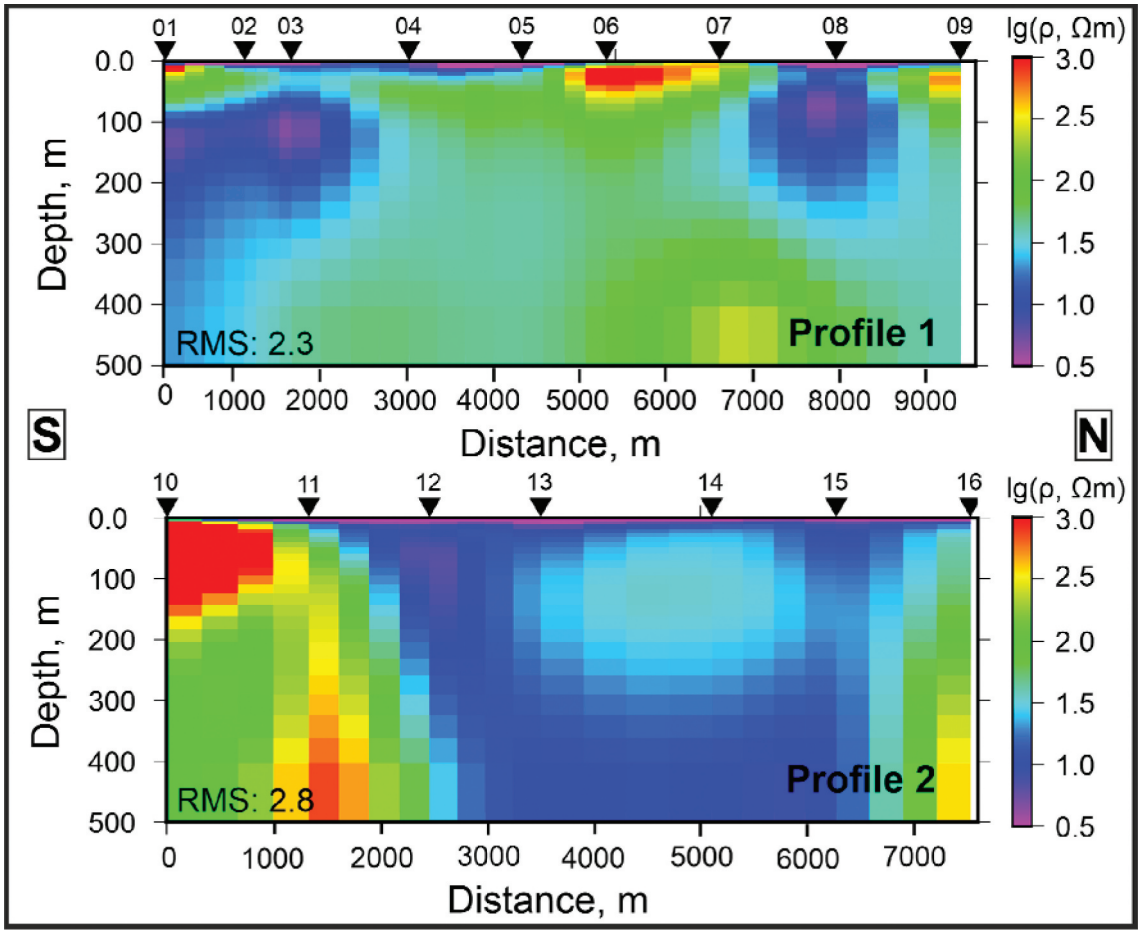

Figure 10. 2D inversion models along profiles 1 and 2.

100 m resistivities was applied. On the apparent resistivity, the error-floor was set at 20%, and it was set at 5% on the impedance phase. After 10 iterations, the mismatch between observed and model response is quantified by the root mean square (RMS) error parameter, which has values of 2.4 and 2.8 for the developed models along profiles 1 and 2, respectively.

The final resistivity 2D models reach depths of 500 m and have resistivity ranges from about 5 to 1000 Ohm.m. Resistivity ranging from 30–100 Ohm. m can be used to perceive and portray subsurface freshwater. The high resistive layers shown in both profiles point to high resistive limestone, which appears clearly in profile 2 below sites 10 and 11. On contrary, the high conductive layers can refer to the existence of clays and shales layers.

5. Discussion and conclusion

The principal target of this study is to map the water bearing formation(s) in the study area and to highlight the structural elements in the area. The results of the integrated interpretation of the data sets of TEM and CSAMT show a good consistency in the conductivity distribution. The results of the cross-sections, which are obtained from both TEM

and CSAMT methods, indicate that two to three geoelectrical layers can be recognised in the subsurface medium.

According to the geoelectrical cross sections, we can conclude the following points:

(1) The subsurface section is composed mainly of a high conductive layer that is mainly clay saturated deposits of Pliocene age with big thickness (~60 m). Certainly, that is more suitable for all kinds of agricultural activities in the area.
(2) There are some lenses of sand deposits embedded in the clay layer. Those can be water bearing lenses, but they are not suitable for any ground water drilling.
(3) At depths of 100 m and more, a moderate resistive layer (20–50 Ohm.m) that represents the Eocene aquifer has a relatively big thickness (up to 300 m) in the study area. The Eocene water bearing formation is the major ground water sources in the studying area.
(4) Some structural elements (faults) are represented along the studied cross-sections. These structures are clear at the abrupt variation of resistivity values in the cross-section.
(5) The water potentiality in the area is situated at two levels (Figure 11):
   a. The first starts just beneath the rock cap at depths over 50 m and nears to 200 m in some places. The charge of this level comes through the captured sand lens content and the draw through the fractures and cracks. A massive bottom closes the water bearer; however, a chain of the inclined fissures and cracks allows the flow of the water into the aquifer as a recharge. Due to the water type, the lateral migration of the Nile water constitutes a considerable portion of the recharge process.
   b. The second level starts at depths around 250 m and extends to 500 m. It is relatively larger in its water content with respect to the first level so that it could be considered as the

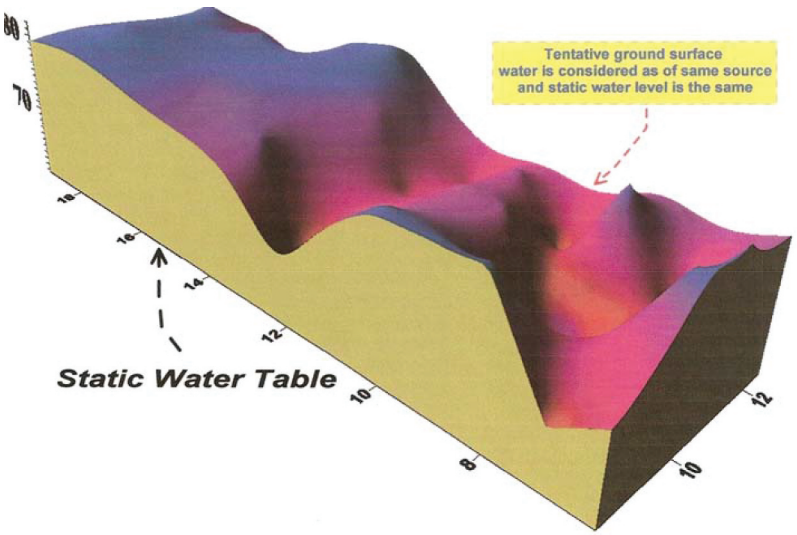

(a)

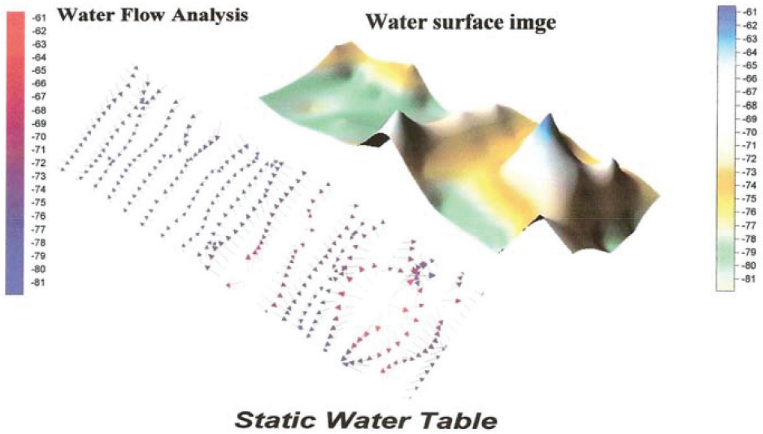

(b)

Figure 11. Static water table at the study area (a) and flow direction (b).

main reserve aquifer for the area. It mainly consists of a series of sub-aquifers that are unconfined in most of their cases. The discharge–recharge regime could be identically defined as discharge towards the first level and as recharge through the third level, the first level and the Nile water.

In conclusion, the top layer is quite thin with a maximum thickness of 10 m and reveals a wide scope of resistivity values (50–200 Ohm.m), indicating the impact of surface conditions and /or lithological varieties. It mainly consists of sand and gravel of the Quaternary age.

The subsequent layer was distinguished as being consecutive underneath all sites over the studied profiles. It reveals low to medium resistivity values and extends to greater depths ranging from 75 m to 100 m below the ground surface. This thick layer may be composed of clay beds intercalated with sand lenses and sand sheets of the Pliocene age. The section has been ended by a relatively resistive layer, which appeared only in profile 1 at a depth of about 75 m below the ground surface. This layer is supposed to be composed of fractured limestone, sand and marl deposits of the Eocene age. It is recommended in the future research to carry out a joint inversion of low frequency mode of MT data to investigate the little deep seated lithostratigraphy of the study area.

Acknowledgements

The authors are very grateful to all researchers of the National Research Institute of Astronomy and Geophysics (NRIAG), who assisted in the acquisition during filed measurements using NRIAG instruments.

Disclosure statement

No potential conflict of interest was reported by the author(s).

ORCID

Hany Shaaban http://orcid.org/0000-0002-1396-8235
Mohamed Abdel Zaher http://orcid.org/0000-0002-4443-4770

References

Abdel Moneim AA, Fernández-Álvarez JP, Ella E.M AE, Masoud AM. 2016. Ground- water management at west el-minia desert area, egypt using numerical modeling. Journal of Geoscience and Environment Protection. 4 (7):66–76. doi:10.4236/gep.2016.47008.

Abou Heleika MM, Niesner E. 2008. Configuration of the limestone aquifers in the central part of egypt using electrical measurements. Hydrogeol J. 17(2):433–446. doi:10.1007/s10040-008-0360-8.

Amato F, Pace F, Vergnano A, Comina C. 2021. TDEM prospections for inland groundwater exploration in semi-arid climate, island of fogo, cape verde. J Appl Geophys. 184:104242. doi:10.1016/j.jappgeo.2020.104242.

Ammar AI, El-Ata AA, Mustafa AA, Lala AMS. 2021. Specifying of aquifer characteristics using forward and inverse modeling of DC-resistivity and TEM methods. Heliyon. 7(5):e06946. doi:10.1016/j.heliyon.2021.e06946.

Bostick FX, 1977. A simple almost exact method of MT analysis, workshop on, electromagnetic methods in geothermal exploration, snowbird, utah, U.S, geol, surv, Contract no, 14080001–8–359.

Buselli G, O'Neill B. 1977. SIROTEM: a new portable instrument for multichannel transient electromagnetic measurements. Explor Geophys. 8(3):82–87. Issue. doi:10.1071/EG977082.

El Ayyat AM. 2021. Facies-based model and basin architecture of the eocene succession in egypt (eastern desert and sinai): an example for tectonically controlled sedimentation on the southern Tethyan margin. Arabian Journal of Geosciences. 14(9):1–31. doi:10.1007/s12517-021-06689-0.

El-Rawy M, Moghazy HE, Eltarabily MG. 2021. Impacts of decreasing nile flow on the nile valley aquifer in el-minia governorate, Egypt. Alexandria Engineering Journal. 60 (2):2179–2192. doi:10.1016/j.aej.2020.12.037.

Fornaciai A, Andronico D, Favalli M, Spampinato L, Branca S, Lodato L,Nannipieri L.2021. The 2004-2005 mt. etna compound lava flow field: a retrospective analysis by combining remote and field methods. Journal of Geophysical Research: Solid Earth. 126(3). e2020JB0 20499

Grimm R, Nguyen T, Persyn S, Phillips M, Stillman D, Taylor T, . . . Sheppard D. 2021. A magnetotelluric instrument for probing the interiors of Europa and other worlds. Advances in Space Research. 68: 2022–2037, COSPAR. Published by Elsevier

Ismail E, Abdelhalim A, Abou Heleika M.2021. Hydrochemical characteristics and quality assessment of groundwater aquifers northwest of assiut district Egypt. Journal of African Earth Sciences, 104260.

Mahmoud HH, Kotb AD, Tawfik MZ. 2021. Application of time domain electromagnetic survey to detect fractured limestone aquifer in desert fringes, west assiut, Egypt. NRIAG Journal of Astronomy and Geophysics. V.10(1): 235-243.

Rigw, Research Institute for groundwater (1992) hydrogeological map of egypt, scale 1:100,000. 2nd Edition, Map Sheet of El-Minia.

Rigw, Research Institute for groundwater (2018). hydrogeological map of egypt, scale 1:100,000. 2nd Edition, Map Sheet of El-Minia.

RIGW/IWACO (1989) Development and management of groundwater resources in the nile valley and delta.

Said R. 1997. The geological evolution of the river nile. Springer-Verlag, Springer, New York, NY.

Shaaban H, El-Qady G, Al-Sayed E, Ghazala H, Taha AI. 2016. Shallow groundwater investigation using time-domain electromagnetic (TEM) method at itay el-baroud nile delta, Egypt. NRIAG Journal of Astronomy and Geophysics. 5(2):323–333. doi:10.1016/j.nrjag.2016.05.004.

Shabana AR. 2010. Hydrogeological studies on the area west deir mouas-mallawi, el-minia governorate, Egypt. Egyptian Journal of Geology. 54:61–78.

Siripunvaraporn W, Egbert G. 2000. An efficient data-subspace inversion method for 2D magnetotelluric data. Geophysics. 65(3):791–803. doi:10.1190/1.1444778.

TEMIXL XL V4 (1996): Temix V.4 user's manual, interprex, p468.

Vozoff K. 1991. The magnetotelluric method. In: Nabighian MN, editor. Electromagnetic methods in applied geophysics. tulsa, oklahoma, society of exploration and geophysics. 2B; p. 641–711.

Ye Y, Du J, Liu Y, Ai Z, Jiang F. 2021. Three-dimensional magnetotelluric modeling in general anisotropic media using nodal-based unstructured finite element method. Comput Geosci. 148:104686. doi:10.1016/j.cageo.2021.104686.

Zhang J, Liu J, Feng B, Guan J, Liu Z. 2021. Three-dimensional magnetotelluric modeling using the finite element model reduction algorithm. Comput Geosci. 151:104750. doi:10.1016/j.cageo.2021.104750.

ZondTEM, 2016. Program for one-dimensional data interpretation of transient electromagnetic method using arbitrary source-receiver configuration (loop/line/dipole) version 5.2.